Published in Tribology International, Elsevier, Vol.65 (2013) p.235–247.
http://dx.doi.org/10.1016/j.triboint.2013.03.017

Roughness Signature of Tribological Contact Calculated by a New Method of Peaks Curvature Radius Estimation on Fractal Surfaces

M. Bigerelle[*1,2], J.M. Nianga[3], D. Najjar[4], A. Iost[4], C. Hubert[1,2], K.J. Kubiak[1,5,6]

[1]*Université de Valenciennes, Laboratoires TEMPO / LAMIH, 59313 Valenciennes Cedex 9, France,*
[2]*PRES Lille Nord de France,*
[3]*Equipe Mécanique des Structures, HEI, 13 Rue de Toul, 59046 Lille Cedex, France,*
[4]*LML, UMR CNRS 8107, F-59650 Villeneuve d'Ascq, Arts et Métiers ParisTech, France,*
[5]*University of Leeds, School of Mechanical Engineering (iETSI), Leeds LS2 9JT, United Kingdom,*
[6]*University of Liverpool, School of Engineering, Liverpool L69 3GH United Kingdom.*
krzysztof@kubiak.co.uk

Abstract

This paper proposes a new method of roughness peaks curvature radii calculation and its application to tribological contact analysis as characteristic signature of tribological contact. This method is introduced via the classical approach of the calculation of radius of asperity. In fact, the proposed approach provides a generalization to fractal profiles of the Nowicki's method [Nowicki B. Wear Vol.102, p.161-176, 1985] by introducing a fractal concept of curvature radii of surfaces, depending on the observation scale and also numerically depending on horizontal lines intercepted by the studied profile. It is then established the increasing of the dispersion of the measures of that lines with that of the corresponding radii and the dependence of calculated radii on the fractal dimension of the studied curve. Consequently, the notion of peak is mathematically reformulated. The efficiency of the proposed method was tested via simulations of fractal curves such as those described by Brownian motions. A new fractal function allowing the modelling of a large number of physical phenomena was also introduced, and one of the great applications developed in this paper consists in detecting the scale on which the measurement system introduces a smoothing artifact on the data measurement. New methodology is applied to analysis of tribological contact in metal forming process.

Keywords: Roughness, friction, curvature radius, fractal, drawing process, surface metrology.

Published in Tribology International, Elsevier, Vol.65 (2013) p.235–247.
http://dx.doi.org/10.1016/j.triboint.2013.03.017

1 Introduction

In general, the physical responses are due to interactions between physical processes and some surface characteristic parameters, such as the geometrical ones, and in particular, the curvature radius from which an estimate could be easily obtained for periodic or stochastic surfaces. However, although its importance is very often underestimated, this one appears in the mathematical formulation of numerous physical models: in optics, it represents a threshold, under which the reflected beam on a surface could not be modelled by the Kirchhoff method, in tribology, it plays an important role in the determination of the contact pressure.

Generally, the calculation of the radius of curvature requires rather smooth curves of studied surfaces, however it is not always the case when dealing with fractal surfaces, as it was shown in Mandelbrot's works [1, 2]. Furthermore, as all the metric parameters relative to a fractal curve depend on the scale of measurement, it thus becomes particularly difficult to give a sense to the notion of local radius of curvature for fractal surfaces. In tribological contact fractal surface are often used to avoid sensibility to scale of measurement [3, 4, 5]. However, some methods thanks to Fourier analysis were proposed with the aim of the estimation of the radius of curvature [6, 7]. Let us note moreover that, for special classes of surfaces, for which the spectrum could be related to the fractal dimension, the curvature radius could be estimated. However, restrictive conditions of surfaces, as the self-affinity, as well as the existence of artifacts in the Fast Fourier Transform, make that method uncertain. Furthermore, the representation of the radius of curvature in the Fourier space has not been extensively studied. Numerous questions arise then: What really the radius of curvature for a fractal curve means? Does it possess a geometrical meaning? What is the interest of its eventual estimation? What could we deduct, from physical models, based on the consideration of such a parameter? All these questions show the necessity to give a geometrical formulation of the curvature radius for a fractal curve. Consequently, in this paper, we suggest establishing, at the same time, the dependence of the radius of curvature on the scale under which the studied surface is observed, as well as, its relation to the fractal dimension of that surface. So, as the properties of the fractal curve are defined from the fractal dimension, the regular non fractal surface is then influenced by the fractal dimension of the studied real surface.

Consequently, even under a formulation supposing regular surfaces, as the physical formulation evoked above, we could not neglect the fractal dimension. To calculate this last one, there are various numerical methods, still not giving the same result, when they are applied to a modelled surface with known fractal dimension. Due to that inconsistency, the method which we should choose is the one presenting the same properties as those of the curves used in the physical model. So, if we want to estimate the influence of the fractal dimension of a surface on the estimation of the radius of curvature, we have to calculate this one, from the last one, with the same scale used for the computation.

This paper is divided into two parts:

In Part I we first review classical methods of calculation of the radius of curvature, and in particular, that of Nowicki's [8] relative to the regular curves, and for which, we proceed to an adaptation, before its extension to fractal curves. Then, we introduce a new calculation approach for the fractal dimension of surfaces. Its accuracy is tested on fractal curves with known fractal dimension, and some mathematical properties of the radius of curvature are stated.

In Part II the proposed method is applied to analysis of tribological contact in metal forming process. Variation of peaks curvature radius before and after the process is revealing detailed topographical signature of different parts of tribological contact. Therefore, the history or contact conditions can be analysed and different zones inside the contact area can be distinguished. We also show that proposed method could be coupled with an inverse methodology to obtain simulated profiles presenting the same morphology as experimental curves measured by tactical profilometer on surfaces obtained by polishing. Next presented application is an analysis of artifacts introduced by radius of tip during measurement of surface by a stylus profiler.

2 Part I – Mathematical model of Curvature Radius of a rough surface

2.1 Model of Curvature Radius

2.2 A Fractal definition of the Curvature Radii of a Surface

Let Γ be the profile of a given rough surface. Γ can be considered as the graph of a continuous function z, defined by

Published in Tribology International, Elsevier, Vol.65 (2013) p.235–247.
http://dx.doi.org/10.1016/j.triboint.2013.03.017

$$\begin{aligned} z : [a,b] &\to IR \\ t &\mapsto z(t) \end{aligned} \quad (a < b), \tag{1}$$

and parameterized by the real variable t, where the parameterization is introduced by the function γ, defined as follows:

$$\begin{aligned} \gamma : IR &\to \Pi \\ t &\mapsto \gamma(t) = (t, z(t)) \end{aligned} \tag{2}$$

(t, z(t)) represents any point of the real plane Π. The curvature $\chi(t)$ of the parameterized curve led by γ, is then defined by:

$$\chi(t) = \frac{|z''(t)|}{|1 + z'^2(t)|^{3/2}} \tag{3}$$

Therefore, the curvature radius r(t) of the profile Γ at the location t, can be written such as: $r(t) = \dfrac{\left(1 + z'^2(t)\right)^{\frac{3}{2}}}{|z''(t)|}$ (4)

with $|z''(t)| \neq 0$ for any $t \in [a,b]$. Consequently, the mean curvature radius of that profile, on the interval $[a,b]$, is then given by: $\bar{r} = \dfrac{1}{b-a} \int\limits_{t \in [a,b]} r(t)\, dt$ (5)

The derivative functions in Eq.3 and Eq.4 are generally estimated by the finite differences method, which is far from being stable. Whitehouse [9] then proposed a better estimation, by using the polynomial interpolation. However, it was established, without using the fractal concept, therefore this method can not be used [10]. Other methods based on the Fourier analysis [11] could be used, but they present the weakness not to be consistent in numerical calculation. For those reasons, Longuet-Higgins [12] proposed a statistical method based, respectively, on the distributions of the maxima and crossings of the mean level, for a random surface, but this method supposes the curvature to be statistically independent of the scanning scale. Whitehouse and Archard [13] then proposed a method using the autocorrelation function to estimate the curvature statistics. That method was subsequently modified by Sales and Thomas, who used the truncated autocorrelation function, according to the Maclaurin series expansions [14] . Moalic *et al*. [10] proposed the application of the finite differences method on the modified autocorrelation function, in order to estimate the repartition of the curvature of the profile. However, the authors found that errors increase with increasing of the wave number. Using now the fractal

Published in Tribology International, Elsevier, Vol.65 (2013) p.235–247.
http://dx.doi.org/10.1016/j.triboint.2013.03.017

approach, Ganti and Bhushan [15] found that the curvature of the profile follows a power-law $\chi(t) \propto f_h^{\Delta}$, where f_h is the Nyquist frequency of the surface, related to the resolution of the instrument, and where the parameter Δ is its fractal dimension. This theory supposes that the spectrum of the surface follows a power law $P(f) \propto f^{2\Delta-5}$, with f_h >>1/L, and where L is the scanning length. However, as noticed by Gallant *et al.* [16] in the context of the estimation of the spectrum, the effect of the smoothing due to the measurement, provides yet another factor which limits the size of the frequency f_h. However, the condition $P(f) \propto f^{2\Delta-5}$ restricts strongly the use of this method, as we could establish it, in the case of a white noise, for which $P(f)$ is constant.

The common point of all these methods is that they are based on statistical, differential or fractal properties, which could be indirectly related to the radius of curvature of the studied profile.

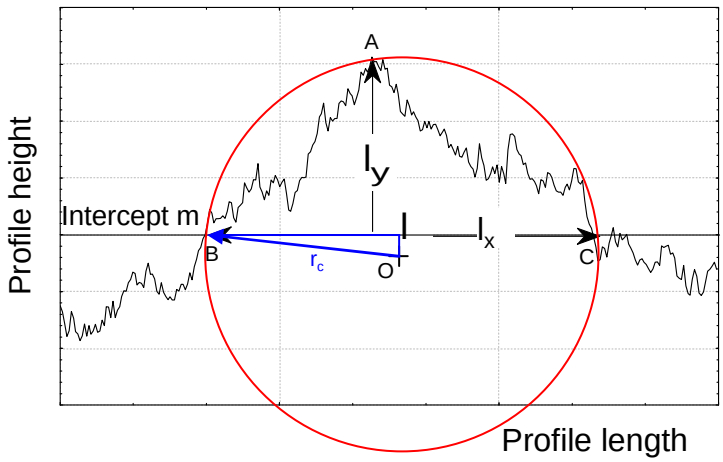

Figure 1: Definition of l_x and l_y used to calculate the local curvature radius $r_c(l_x)$.

However, contrary to the previous ones, the method proposed by Nowicki [8] allows the study of the surface roughness, by introducing a parameter, directly measured from the surface: the so-called, radius of asperity (Figure 1), defined as follows:

$$r_c = l_x^2 / 8 l_y \qquad (6)$$

with $l_y = 0.1 R_{max}$ or $l_y \approx 0.05 R_{max}$, and where R_{max} is the maximal range amplitude of the profile. This method consists in finding the radius r_c of a circle of canter O,

passing by a crest A, and by two other points B and C of the profile; these two last ones being distant of l_x. The distances which separate the line (B, C), respectively from A and from O, are l_y and r-l_y The parameter l_y is considered sufficiently small, so that the segment [A, O] is supposed to be perpendicular to [B, C], in its middle I. If we now apply Pythagoras' theorem to the triangle OBI, it then follows:

$$\left(l_x / 2\right)^2 + \left(r_c - l_y\right)^2 = {r_c}^2 \tag{7}$$

Consequently, we get:

$$r_c = \frac{l_y}{2} + \frac{l_x^2}{8 l_y} \tag{8}$$

Eq. (8) is obtained, assuming that l_y is sufficiently small, and the following condition is satisfied:

$$l_y < l_x \tag{9}$$

Nevertheless, some remarks can be drawn for such a method:

I) The techniques to detect the peaks are not well defined. So, when l_y value is fixed, Nowicki's method determines all local peaks (in a discretized case, if $z_{i-1} < z_i$ and $z_i > z_{i+1}$, then z_i corresponds to a peak). In what precedes, it is assumed a uniform partition of the interval [a, b], with a grid $t_0 < ... < t_{i-2} < t_{i-1} < .... < t_N$, and with $z_i \simeq z(t_i), i = 1,2,...,N$. Then, as l_y values are fixed, there exists for each peak, a unique value of l_x giving the following discretized set $\left\{z_{i-q},...,z_{i-1},z_i,z_{i+1},z_{i+2},...,z_{i+p}\right\}$. The peak is retained if $z_{i-q} < ... < z_{i-2} < z_{i-1} < z_i$ and $z_i > z_{i+1} > z_{i+2} > ... > z_{i+p}$. This local radius curvature will be named Euclidian Radii Curvature with the following notation $\tilde{r}_i(t_i)$. On the other hand, the analytical method supposes that z_i is the maximal peak of the non-discretized surface, and implies $p = q,$ if the peak gets a perfect circular shape. Reciprocally, if $p \neq q,$ this last one does not get such a shape.

II) The threshold used to estimate $l_y = \alpha R_{\max}$ does not have any theoretical justification. Indeed, trying to determine the parameter radius of the crest, we have $l_y = \lim_{\alpha \to 0} \alpha Rt$. However, on discretized curves and for l_y sufficiently small, the choice

of l_x becomes indeterminate, due to the fact that $l_x = k\,\delta_x$, where δ_x is the length of the sampling interval. Furthermore, because of the stochastic aspect of the profile, the three points A, B and C become more and more aligned, when the value of l_x is decreasing, implying a dramatic increasing of the r_c variance estimator.

III) On experimental profiles, a smoothing effect is realized under a characteristic length [17]. For example, if the profile is recorded by a tactile profiler, the recording surface is then seen smoother at a length of the same order of magnitude than the tip curvature radius. Consequently, for l_y sufficiently small, one has to record the curvature radius of the measurement artefacts, and the curvature radii will then be wrongly increasing.

IV) If the surface contains some noise (white or pink), there exists a great probability for the Nowicki's algorithm to detect false peaks. Finally, the Radii of curvature get erroneous.

V) If the profile is the result of the combination of different processes acting at various scales, the radii of curvature so obtained are different. However, it becomes evident that the detection of peaks becomes uncertain and will so favour smaller peaks.

VI) For physical surfaces possessing a fractal aspect [18, 19, 20, 21], the calculation of r_c has no physical sense and the Nowicki's method will lead to different values of that parameter, depending on the sampling rate. Furthermore, it is noticed that the decreasing of the sampling rate will decrease $\tilde{r}_c$. This confirms that $\tilde{r}_c$ calculated by the Nowicki's method have no sense if we postulate that $z_{i-q} < \ldots < z_{i-2} < z_{i-1} < z_i$ and $z_i > z_{i+1} > z_{i+2} > \ldots > z_{i+p}$ (see appendix A for more detailed justification).

2.2.1 Theoretical relation in proposed method

For fractal curves, r_c depends on the scale at which the observation is made. And, as we postulate that the curvature radii could be defined at a given scale, the Nowicki's method has then to be reformulated. We will conserve the notion of l_x without imposing any property to the points of the profile that are related to it, since α cannot be fixed without introducing an artefact. For these reasons, we choose to calculate l_x by the following method:

1) We choose a horizontal straight line at the level *h* that crosses the profile, and we built a set of l_x values intercepting the profile. More precisely, $z_i < h,\ \ j \geq 1,\ \ (z_{i+1}, z_{i+2}, \cdots, z_{i+j}) \geq m,\ \ z_{i+j+1} < m,\ \ l_x = x_{i+j+1} - x_i$ where m is a number of intercepting horizontal lines used in algorithm that are uniformly randomly chosen.

2) For each l_x, the local maximal peak (maximum value of profile) is obtained which gives l_y. More precisely,

$$z_i < h,\ \ j \geq 1,\ \ (z_{i+1}, z_{i+2}, \cdots, z_{i+j}) \geq m,\ \ z_{i+j+1} < m,\ \ l_y = \sup_{k \in \{i+1, i+2, \cdots i+j\}} (z_k) - h$$

3) r_c is then computed from Eq.6, and this process is repeated for all the other elements of the set of l_x values.

4) Another horizontal straight line is chosen randomly and the steps 1 to 3 are repeated.

The detailed algorithm is presented in Figure 2.

Published in Tribology International, Elsevier, Vol.65 (2013) p.235–247.
http://dx.doi.org/10.1016/j.triboint.2013.03.017

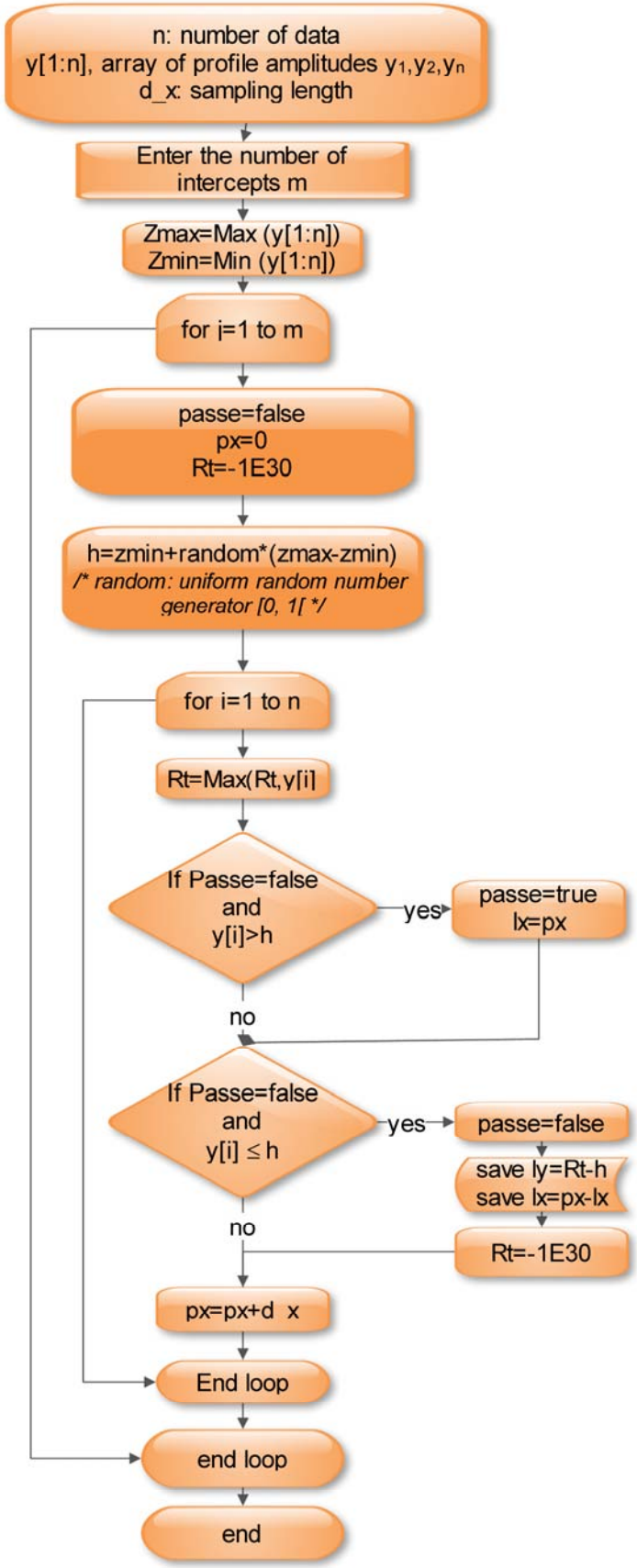

Figure 2: Algorythm used to calculate the Curvature Radius Estimation on Fractal Surface.

Published in Tribology International, Elsevier, Vol.65 (2013) p.235–247.
http://dx.doi.org/10.1016/j.triboint.2013.03.017

Theorem 1: If l_x exists, for all non-constant continuous function f uniformly Hölderian, anti-Hölderian, and defined on a real interval $[a,b]$, one gets, for the fractal dimension of the graph G_f of f :

$$\Delta(G_f) = \limsup_{l_x \to 0} \left(\log r_c(l_x) / \log l_x \right) \tag{10}$$

Rationalization of the approach: As f is Hölderian in *t,* with exponent H ($0 < H \le 1$), there exists a positive constant c, such that, for any t' :

$$\left| f(t) - f(t') \right| \le c \left| t - t' \right|^H \tag{11}$$

Eq.11 follows Hölderian form: [22]

$$v(t,\varepsilon) = \sup_{t',t'' \in [t-\varepsilon, t+\varepsilon]} \left| f(t'') - f(t') \right| \le c(t)\varepsilon^H \tag{12}$$

Then if f is uniformly then the constant c is independent of t, by integration over the domain of definition T, $\bar{v}(T,\varepsilon) = \int_T \sup_{t',t'' \in [t-\varepsilon, t+\varepsilon]} \left| f(t'') - f(t') \right| dt \le c\varepsilon^H$ (12)

with $\Delta(G_f) \le 2 - H$ (13)

On the other hand, as f is uniformly anti-Hölderian too, with the same exponent, there exists a positive constant c', independent of t such that, for any ε :

$$\bar{v}(T,\varepsilon) \ge c'\varepsilon^H \tag{14}$$

With $\Delta(G_f) \ge 2 - H$ (15)

Taking (12) and (14) into account, we can then write, for ε taking the particular value $\frac{l_x(t,h)}{2}$ at the level h that crosses the profile (the term 1.2 is due to the fact that $v(t,\varepsilon)$ is defining on a 2ε interval from Eq.12):

$$c(t)\left(\frac{l_x(t,h)}{2} \right)^H \ge v\left(t, \frac{l_x(t,h)}{2} \right) \ge c'(t)\left(\frac{l_x(t,h)}{2} \right)^H \tag{16}$$

$\sup_{t',t'' \in [t-\varepsilon, t+\varepsilon]} \left| f(t'') - f(t') \right|$ from Eq.12 is the local range of the function and is identified with the height $l_y(t,h)$ of the peak of width $l_x(t,h)$, localized in t according to our definition.

Then $v(t,\varepsilon) = l_y\left(\frac{l_x(t,h)}{2}, t \right)$ and one gets:

Published in Tribology International, Elsevier, Vol.65 (2013) p.235–247.
http://dx.doi.org/10.1016/j.triboint.2013.03.017

$$c(t)\left(\frac{l_x(t,h)}{2}\right)^H \geq l_y\left(\frac{l_x(t,h)}{2},t\right) \geq c'(t)\left(\frac{l_x(t,h)}{2}\right)^H \quad (17)$$

But, f being uniformly Hölderian, then c and c' do not depend on *t,* and therefore [22]:

$$\Delta(G_f) = 2 - H \quad (18)$$

And summing the same $l_x(t,h) = l_x$ with h values defined in $h \in \left[\inf_{t\in[T]} f(t), \sup_{t\in[T]} f(t)\right]$ and $t \in [0,T]$, defining a 2D domain $\Omega(l_x)$ with a $A(\Omega(l_x))$ area (in case of discreet set of measured profile points $A(\Omega(l_x))$ is the size of this set), then :

$$c \iint_{\omega\in\Omega(l_x)} \left(\frac{l_x(t,h)}{2}\right)^H d\omega \geq \iint_{\omega\in\Omega(l_x)} l_y\left(\frac{l_x(t,h)}{2},t\right) d\omega \geq c' \iint_{\omega\in\Omega(l_x)} \left(\frac{l_x(t,h)}{2}\right)^H d\omega$$

and from Eq.12 and Eq.14

$$c\,A(\Omega(l_x))\left(\frac{l_x}{2}\right)^H \geq \iint_{\omega\in\Omega(l_x)} l_y\left(\frac{l_x(t,h)}{2},t\right) d\omega \geq c' A(\Omega(l_x))\left(\frac{l_x}{2}\right)^H$$ that can be rewritten by the practical forms $$c\left(\frac{l_x}{2}\right)^H \geq \frac{1}{A(\Omega(l_x))} \iint_{\omega\in\Omega(l_x)} l_y\left(\frac{l_x(t,h)}{2},t\right) d\omega \geq c'\left(\frac{l_x}{2}\right)^H \quad (19)$$

where $\frac{1}{A(\Omega(l_x))} \iint_{\omega\in\Omega(l_x)} l_y\left(\frac{l_x(t,h)}{2},t\right) d\omega$ represents the mean of all highest peaks of l_x width and is noted $l_y(l_x,T)$.

Then from the definition of the fractal dimension related to the holder exponent [22], it can be noted that $H \approx \log l_y / \log l_x$ and therefore from Eq. 18 we can write

$$\Delta(G_f,T) = 2 - \log l_y(l_x,T) / \log l_x \quad (20)$$

Now if $l_y(l_x,T) << l_x$ then $l_y(l_x,T) = l_x^2/8r_c(l_x,T)$ and we obtain the final result

$$\Delta(G_f,T) = 2 - \left(\log r_c(l_x,T)/\log l_x\right). \quad (21)$$

Remarks.

Experimentally, the fractal dimension $\Delta(G_f)$ is obtained as a slope, by fitting in a log-log plot the discretized data $\left(\log l_x, \log r_c(l_x)\right)$ performed by our algorithm. If the regression line fit well, the experimental data then allow writing:

Published in Tribology International, Elsevier, Vol.65 (2013) p.235–247.
http://dx.doi.org/10.1016/j.triboint.2013.03.017

$$r_c\left(l_x\right) = \alpha\, l_x^{\Delta} \tag{22}$$

So, the relation between l_x and l_y becomes:

$$l_y\left(l_x\right) = \beta\, l_x^{2-\Delta}, \quad \beta = 1/8\alpha \tag{23}$$

An interesting properties linked to the fractal concept is the box counting method. More precisely, the box counting is a method of gathering data for analyzing complex patterns by breaking a dataset, object, image, etc. into smaller and smaller pieces, typically "box"-shaped, and analyzing the pieces at each smaller scale. When box counting is done to determine a fractal dimension known as the box counting dimension, the information recorded is usually either yes or no as to whether or not the box contained the curve or not. In our cases, we will apply similar method counting the circles. We will count the number of cases $N\left(r_c\left(l_x\right)\right)$ when the radius of $r_c\left(l_x\right)$ is met for a given l_x. This expression allows us to quantify the density of peaks of the surface that is fundamental in tribology (contact mechanic, wear,…). However, the density of peaks depends also on the scale. Intuitively, for a fixed macroscopic area, the number of peaks will decrease when their radius will increase. It becomes then obvious to find the scaling law of this decrease. On the other hand, introducing the number $N\left(r_c\left(l_x,T\right)\right)$ of cases where a radius $r_c\left(l_x,T\right)$ on the profile length is met through the above algorithm (of this is the same number of count that $l_y\left(l_x,T\right)$ i.e. $N\left(r_c\left(l_x,T\right)\right) = N\left(l_y\left(l_x,T\right)\right)$). We have found the following results:

$$\Delta\left(G_f,T\right) = \limsup_{l_x\to 0}\left(-\frac{\log N\left(l_y\left(l_x,T\right)\right)}{\log l_x}\right) \tag{24}$$

and therefore $\Delta\left(G_f,T\right) = \limsup_{l_x\to 0}\left(-\frac{\log N\left(r_c\left(l_x,T\right)\right)}{\log l_x}\right)$ (25)

The same reasoning as for Eq.22 and Eq.23 applied to Eq. (24) and Eq. (25), allows us to obtain the following power laws:

$$N\left(r_c\left(l_x\right)\right) = \alpha'\, l_x^{-\Delta} \tag{26}$$

$$N\left(l_y\left(l_x\right)\right) = \alpha'\, l_x^{-\Delta} \tag{27}$$

Published in Tribology International, Elsevier, Vol.65 (2013) p.235–247.
http://dx.doi.org/10.1016/j.triboint.2013.03.017

2.2.2 Properties

1) The fractal dimension is unchanged if *f* is multiplied by a given factor.

2) The fractal dimension is unchanged, through an γ homothetic transform (i.e. $z' = f(\gamma t)$) of the parameter *t*.

3) If m and m' denote respectively the numbers of z and z' intercepts, with m'=km, then $N\left(r_c\left(z', x\right)\right) = k\alpha' l_x^{-\Delta}$.

4) If we do not impose the conditions $z_{i-q} < \ldots < z_{i-2} < z_{i-1} < z_i$ and $z_i > z_{i+1} > z_{i+2} > \ldots > z_{i+p}$, the Nowicki's method is then a particular case of our method, by taking different values $l_y = 0.1 R_m$.

2.3 Analysis of discretisation error by simulation of Brownian profile

A Brownian profile with fractal dimension 1.5 is generated by an algorithmic process (Figure 3) and discretized in 10^7 points. An advantage of this type of profile is to avoid the arithmetic error due to the floating point and inherent to fractal functions as Knopp or Weierstrass.

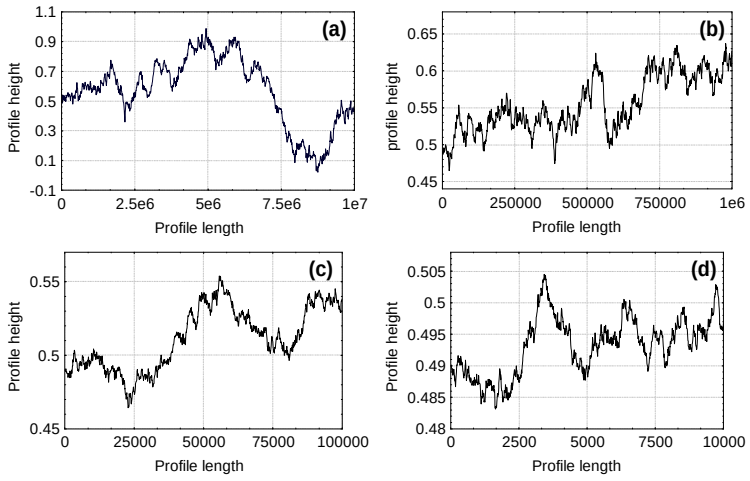

Figure 3: Brownian profile generated using 10^7 discretisation points (a) and different zooms at the origin: x10 (b), x100 (c), x1000 (d).

The sampling rate is equal to 1 meaning that $x_{i+1} - x_i = 1$ and the profile is normalised to an amplitude equal to 1 on the whole interval length L. As it was proved, these operations do not affect the different values of the signal fractal dimension. When the algorithm is applied on curves with a number of intercepted lines m=100 (Figure 1),

Published in Tribology International, Elsevier, Vol.65 (2013) p.235–247.
http://dx.doi.org/10.1016/j.triboint.2013.03.017

one obtains a total of 94026 couples of values $\left(l_x, l_y\left(l_x\right), r_c\left(l_x\right)\right)$ where $l_x \in \left[1 \cdots 8745294\right]$. As a result of the computation, the variation ranges for $l_y\left(l_x\right)$ and $r_c\left(l_x\right)$ are respectively $\left[3.83\,10^{-9} \cdots 0.99\right]$ and $\left[467 \cdots 1.110^{13}\right]$. As l_x values integers on account of the discretization and according to Eq. 10, one gets a set of values $r_c\left(l_x\right)$ and $l_y\left(l_x\right)$ for a given l_x. However, if we plot the graph of the set $\left(l_x, l_y\left(l_x\right), r_c\left(l_x\right)\right)$ and determine the fractal dimension, the slope of the regression line will then be calculated for a great part of the small l_x values. If we make the regression from the set of data, one can obtain $N\left(l_y\left(l_x\right)\right) = N\left(r_c\left(l_x\right)\right) = 30902\, l_x^{-1.42}$ (Figure 4) with a good coefficient of correlation r = 0.98.

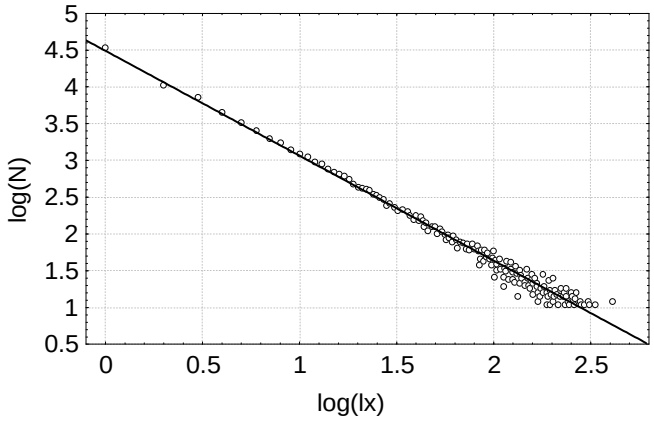

Figure 4: Evolution of the number of curvature radii $\log N\left(r\left(l_x\right)\right)$ of the profile shown in Figure 3a, estimated at a l_x values versus the $\log l_x$ value.

Consequently, we decide to calculate the value of the mean $\left(\overline{l_y}\left(l_x\right), \overline{r_c}\left(l_x\right)\right)$, for each l_x. Figure 5a represents the variation of $\log \overline{r_c}\left(l_x\right)$ versus $\log l_x$ and the corresponding linear equation is given by:

$$\log r_c\left(l_x\right) = 2.756_{\pm 0.01} + 1.488_{\pm 0.004} \log l_x \qquad (28)$$

with regression coefficient r=0.998. The studied test proves that this slope is not statistically different from the theoretical fractal dimension equals to 1.5 for the Brownian motion. Four remarks could then be stated from the analysis of the residual regression:

Published in Tribology International, Elsevier, Vol.65 (2013) p.235–247.
http://dx.doi.org/10.1016/j.triboint.2013.03.017

i) $r_c(l_x)$ is overestimated for small l_x values and increases exponentially with l_x: there are estimation errors on $r_c(l_x)$.

ii) The l_x are approximately Gaussian distributed values with a high right tail.

iii) The $r_c(l_x)$ dispersion increases with l_x.

iv) The linear approximation is accurate for the values of l_x that are not too small.

The appendix B presents other validations with function possessing different fractal dimensions.

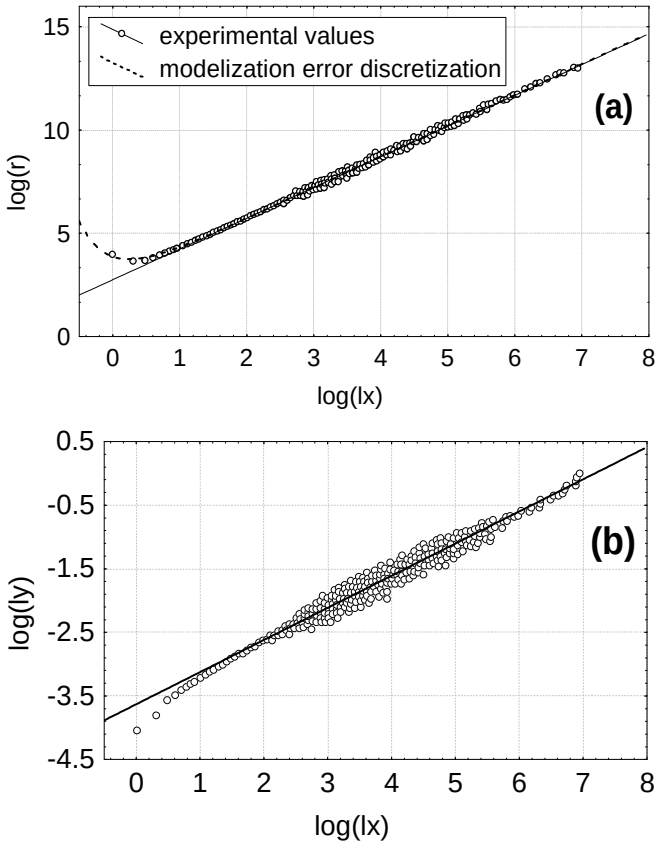

Figure 5: Evolution of the curvature radius $\log r(l_x)$ of the profile shown in Figure 3a, estimated at a l_x values versus the $\log l_x$ value (a). The thin line corresponds to the equation $\log r_c(l_x) = 2.756_{\pm 0.01} + 1.488_{\pm 0.004} \log l_x$ and the dashed one to the corrected method with $\log r_c(l_x) = 2.732_{\pm 0.01} + 1.494_{\pm 0.003} \log l_x + 1.14_{\pm 0.1} / (n_x - 1)$ (where n_x is the number of d_x intervals used to calculate l_x). The graph (b) represents the evolution of the height curvature radii $\log l_y(l_x)$ versus the $\log l_x$ value.

Published in Tribology International, Elsevier, Vol.65 (2013) p.235–247.
http://dx.doi.org/10.1016/j.triboint.2013.03.017

3 Part 2 – Model application to physical processes

3.1 Example 1 – Analysis of peaks radius flattening during boundary lubricated friction

3.1.1 Metal forming experimental device

Experimental analysis of aluminium strip reduction by drawing process has been carried out using device developed by Bech et al. [23] at Technical University of Denmark. It consist of two working tools, i.e. glass and steel dies rigidly mounted in experimental setup assuring 20% reduction in thickness of aluminium strip. Steel die is inclined of $\beta=3°$ and its position is adjusted so that deformatio n zone can be observed through die made of transparent hardened glass. Glass die is in form of circular disc with 50 mm diameter and 11 mm thick. The drawing speed V_s can be adjusted and in this study speed of 5 mm/s has been used. Schematic diagram of experimental device is presented on Figure 6. The material used for strip is semi-hard aluminium AISI 1050 H24. The strips have been cut from a metal sheet of 2 mm into samples of the following dimensions: 450 x 20 x 2 mm. One side of the strip have been textured. Mesoscopic pockets were manufactured using Electro Discharge Machining (EDM) technique. Pockets in shape of about 10 x 2 mm grooves were manufactured, initial angle of side walls creating the pockets were about $\alpha_o = 10°$. Initial roughness inside the pockets were significantly higher than roughness on flat surface between the pockets (Figure 7). Viscosity of used mineral oil was 0.5954 Pa·s.

Published in Tribology International, Elsevier, Vol.65 (2013) p.235–247.
http://dx.doi.org/10.1016/j.triboint.2013.03.017

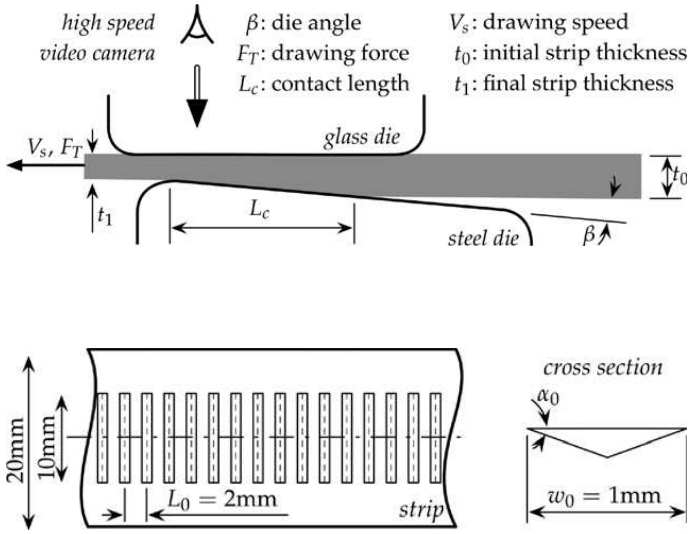

Figure 6: Schematic diagram of experimental device used for drawing process [after 24].

3.1.2 Surface roughness measurement and analysis

Surface roughness were measured using Zygo NewView 7300 interferometric profiler. Vertical Scanning Interferometry (VSI) was used to measure the surfaces. The measurement principle is that unfiltered white light beam is split in two. Half of a beam is directed through a microscope objective and reflected from the surface and half is reflected from the reference mirror. When reflected beams combine together they produce interference fringes, where the best-contrast fringe occurs at best focus. In VSI mode the objective moves vertically to scan the surface at various heights. A 3D surface is reconstructed by analysis of fringes at every pixel. VSI mode uses algorithm to process fringe modulation data from the intensity signal to calculate surface heights. Obtained resolution will therefore depend on a precision of z axis positioning. In case of Zygo NewView 7300 instrument a piezoelectric stage with range of 160 µm is used to refine the height resolution going down to less than a 1 nm. Spatial resolution will depend on camera size and used objective. In our case a several scans were made and stitched together to cover an area of 2 x 8 mm with spatial resolution (X, Y) resolution of 1.1 µm.

Published in Tribology International, Elsevier, Vol.65 (2013) p.235–247.
http://dx.doi.org/10.1016/j.triboint.2013.03.017

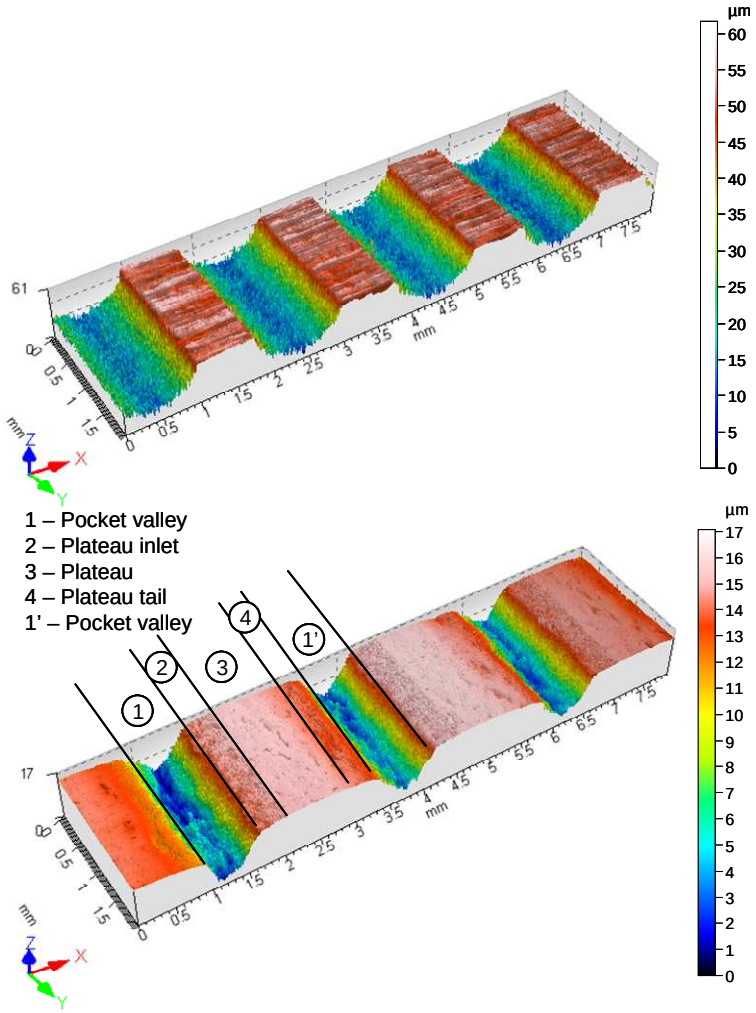

Figure 7: Initial textured surface with pockets prepared by electro erosion process and final morphology after drawing test, lubricated by mineral oil, different zones created on textured surface can be defined.

On the surface measured after the lubricated drawing test has been performed, different zones on tribological contact can be defined. As shown on Figure 7 on both sides of deformed plateau two new zones can be found: zones 2 and 4. Initially those surfaces were inside the cavities pockets and due to elastoplastic deformation they form now part of a plateau. However, due to contact lubrication there was only partial contact between plateau and glass tool. In such contact, surface roughness will change leaving a specific signature of tribological process. Analysis of surface roughness can reveal that signature. However, direct analysis of 3D surface morphology is computationally more expensive and less robust than 2D analysis. Therefore to analyse surface roughness specific technique of transition from 3D surface to 2D surface profiles analysis has been developed. It consist of generation a

Published in Tribology International, Elsevier, Vol.65 (2013) p.235–247.
http://dx.doi.org/10.1016/j.triboint.2013.03.017

series of 2D profiles in vertical direction (Figure 8) from 3D surface. Once the profile are extracted different parameters can be calculated from individual profiles. Evolution of that parameters can be plotted in function of initial position of extracted profiles. Hence, every point on a graph corresponds to roughness parameter calculated from one vertical profile (Figure 8).

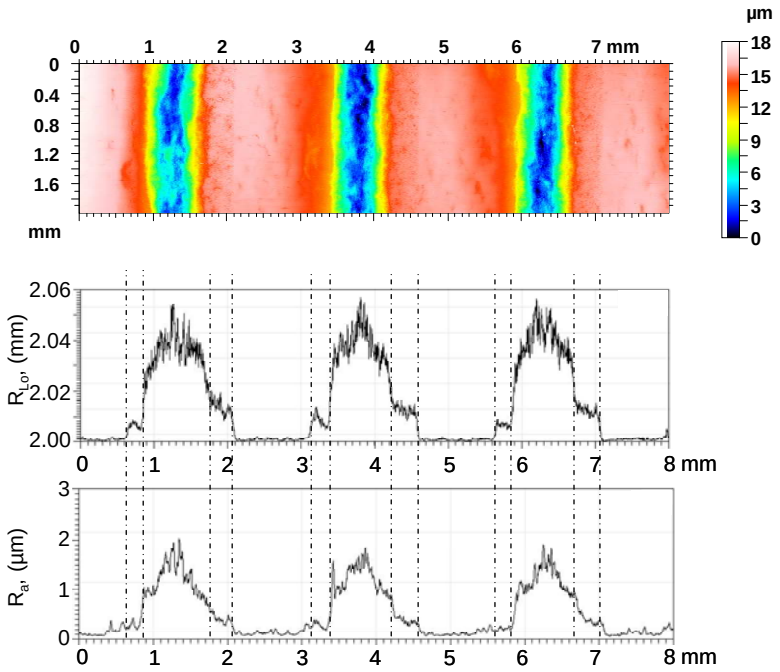

Figure 8: Analysis of roughness parameters (R_a and R_{Lo}) calculated on individual 2D profiles extracted from surface in vertical direction, every point on bottom graphs corresponds to roughness parameter calculated from one vertical profile from surface on top.

Analysis of several different roughness parameters, revealed that only two parameters are able to clearly distinguish created zones on tested surface. The first one is developed length of the roughness profile R_{Lo} (Figure 8) and the second is our new parameter of profile curvature radius r_c (Figure 9 and Figure 10). In this example the r_c is calculated as an average value of r_c and will be named $\overline{r_c}$ for randomly chosen l_x lines. This approach will produce single parameter r_c which will be scale independent. One characteristic value of r_c start to dominate, therefore sufficient sampling number should be chosen to obtain more accurate estimation of dominant curvature radius for a given surface profile. Evaluating the value of $\overline{r_c}$ before and after tribological process create characteristic signature of surface.

For comparison also an evolution of arithmetic mean value of roughness profile R_a has been plotted however zones 2 and 4 can not be distinguished using this simple

Published in Tribology International, Elsevier, Vol.65 (2013) p.235–247.
http://dx.doi.org/10.1016/j.triboint.2013.03.017

amplitude parameter. R_{Lo} is able to show zones 2 and 4 however contrary to r_c the value at the plateau do not present any variation. In Figure 9 an initial value of r_c parameter calculated on initial surface is analysed. Presented in Figure 10 evolution of parameter r_c shows very well different zones and also variations of the parameter across the zone. High value of curvature radius of roughness profile at the left hand side of the plateau (zone 3) confirm more severe contact conditions in this area and flattening of the peaks.

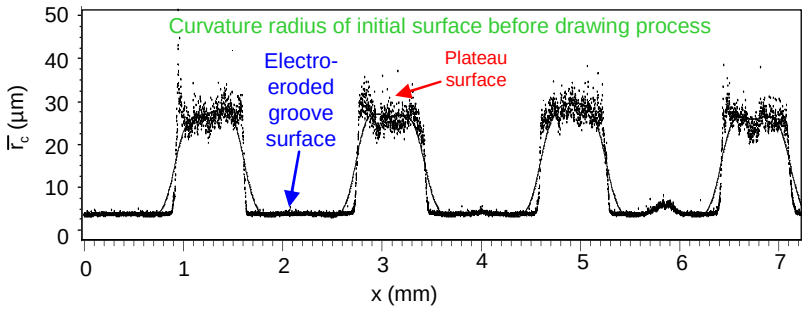

Figure 9: Averaged curvature of peaks roughness $\overline{r_c}$ calculated on initial profile before drawing process, showing very regular sharp peaks in elecroeroded zone (small $\overline{r_c}$ around 6 µm) and higher peaks value on plateau ($\overline{r_c}$ around 30 µm).

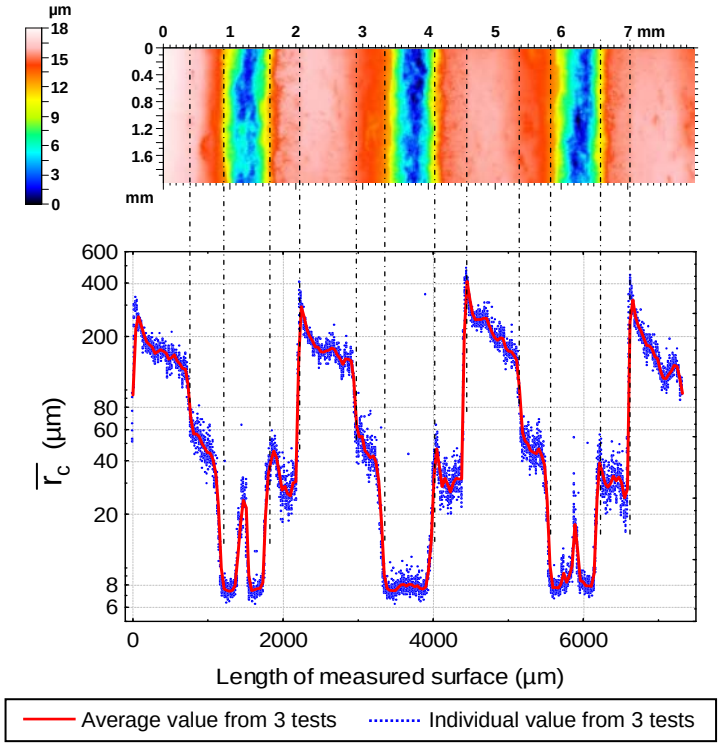

Figure 10: Analysis of average roughness peaks curvature radius ($\overline{r_c}$) calculated on individual 2D profiles extracted from surface in vertical direction, every point on bottom graphs corresponds to roughness parameter calculated from one vertical profile.

Published in Tribology International, Elsevier, Vol.65 (2013) p.235–247.
http://dx.doi.org/10.1016/j.triboint.2013.03.017

Variation of average roughness curvature before (Figure 9) and after (Figure 10) drawing process can be considered as characteristic signature of tribological contact.

3.1.3 Multiscale decomposition

In this section the multiscale decomposition of the radius curvature analysis is performed. One of the major interest in our method is to presents a multiscale evaluation of the radii curvature. As claimed in this paper, the curvature radius depends on the scale. It could then be obvious to represents the effect of drawing conditions as the multiscale variation of the radius curvature.

According to eq. 22 and using a new notation involved by our study, radius curvature is equals to $r_c\left(l_x,p\right)=r_{c0}\left(p\right)\left(l_x\left(p\right)/l_x^0\right)^{\Delta(p)}$ where p represents the position on the measured surface along the drawing direction, l_x^0 the sampling length unit. In this case $r_{c0}\left(p\right)$ can be seen as an unscaled curvature radius i.e. independent of the length $l_x(p)$. The Figure 11 presents the evolution of $r_{c0}\left(p\right)$ and Figure 12 shows evolution of $\Delta(p)$. Therefore, presented in Figure 13 multiscale variogram shows multiscale decomposition like those met in the wavelet decomposition allowing visualizing all multiscale features of the radius curvature. More detailed analysis of those aspects will be published in a follow-up paper where different drawing conditions will be analysed.

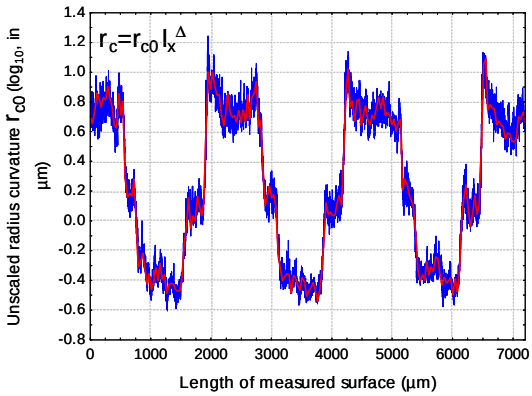

Figure 11: Evaluation' of the unscaled curvature radius $r_{c0}\left(p\right)$ versus the measured surface along the drawing direction p.

Published in Tribology International, Elsevier, Vol.65 (2013) p.235–247.
http://dx.doi.org/10.1016/j.triboint.2013.03.017

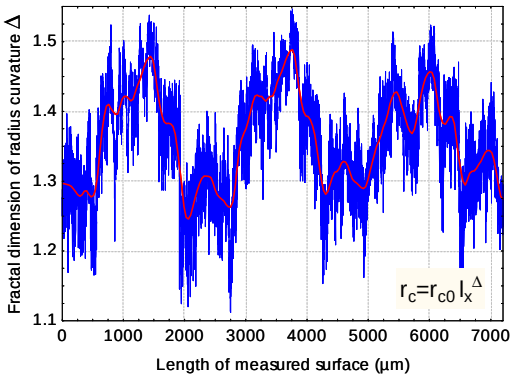

Figure 12: Evaluation of the fractal dimension $\Delta(p)$ versus the measured surface along the drawing direction p.

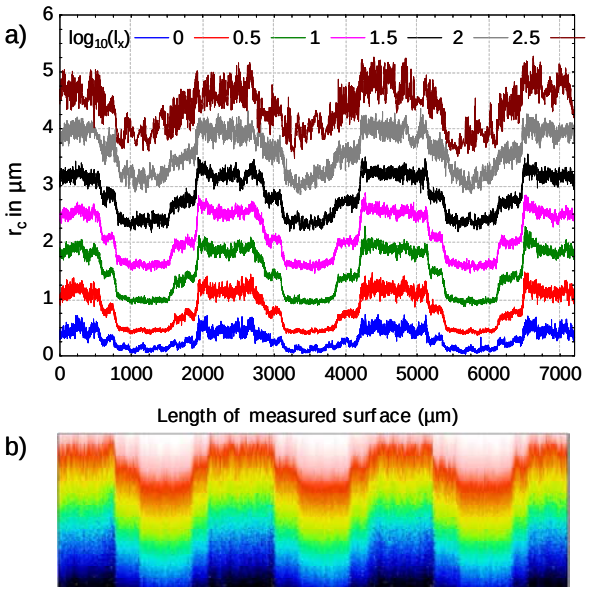

Figure 13: Multiscale decomposition of $r_c\ (l_x, p)$, a) decomposition graph, b) decomposition map.

Different part of surface depending on local contact conditions will have different value of r_c, fractal dimensions and unscaled radius curvatures. In case when the contact conditions are unknown, this parameter can be used to determine the regime of lubrication or zones of direct contact between contacting surfaces. Therefore, it can be a very robust tool for contact rheology by roughness analysis in tribological applications.

3.2 Example 2 – Analysis of stylus tip artifacts introduced during surface measurement

Surface data of a fractal nature may be gathered in a very wide variety of ways. All involve a certain amount of smoothing or degradation of the true surface data according to the recording method. In laser profilometry, devices provide a smoothing measuring the surface height via the interference patterns of the reflected height from a narrow beam. With mechanical profilers, the stylus tip curvature radius makes a smoothing effect on the surface and the information narrower than the stylus tip cannot be recorded. Since the smoothing effect is highly non-linear, it becomes very hard to estimate it on the original data. The basic idea we propose in this paper is to apply the theory of curvature radius to detect the scale on which the measurement system introduces a smoothing artefact on the data measurement. In fact, the smoothing effect will increase the curvature radius on the scale measurement.

3.2.1 Analysis of an experimental measurement

In a great number of roughness study using tactile profilometry, it was shown that the curvature radius r_c calculated from the Nowicki's formulation was not a discriminate parameter for physical phenomena. We also have noticed that the values of r_c will depend on the sampling length. As an application, a pure Aluminium sheet is polished with different paper grades: 80, 120, 220 and 500. Then 30 bi-dimensional profiles are recorded using a tactile profiler with a 10 µm stylus radius.

Figure 14 shows the variation of $\log r_c(l_x)$ versus $\log l_x$ and Figure 15a shows an example of a grade 500 polished surface. As it could be shown on this last one, a cross over appears around $r_c(l_x) = 10\,\mu m$. Below this critical value, $r_c(l_x)$ seems to be constant and over it, $r_c(l_x)$ follows the power law given by Eq. 22. As it could be observed, the curvature radius is lower than for a smaller grain size. For different paper grades, the cross over related to $r_c(l_x)$ is the same but the abscissa l_x increases with the grain size. This fundamental relation shows that whatever the roughness amplitude of polished surfaces (R_a varying from 1.66 µm to 0.02 µm), the stylus size effect will give a same constant value of the curvature radius. The stylus size effect is greatly discussed in the bibliography [25, 26, 27, 28, 29], however no invariance parameter was found in the roughness measurement until now.

Published in Tribology International, Elsevier, Vol.65 (2013) p.235–247.
http://dx.doi.org/10.1016/j.triboint.2013.03.017

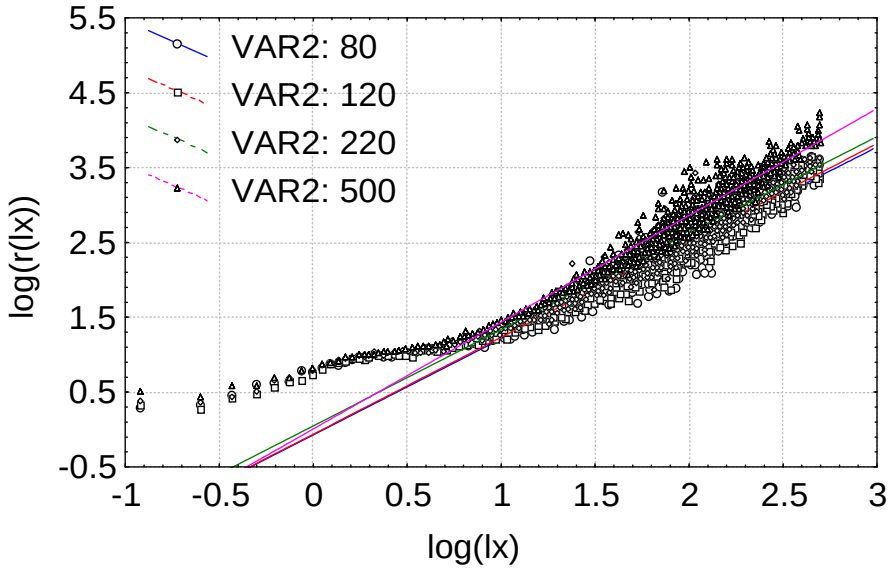

Figure 14: Evolution of the curvature radius $\log r\left(l_x\right)$ versus $\log l_x$ for pure Aluminium sheet surface polished with different paper grades 80, 120, 220 and 500 (l_x and $r(l_x)$ in µm).

Published in Tribology International, Elsevier, Vol.65 (2013) p.235–247.
http://dx.doi.org/10.1016/j.triboint.2013.03.017

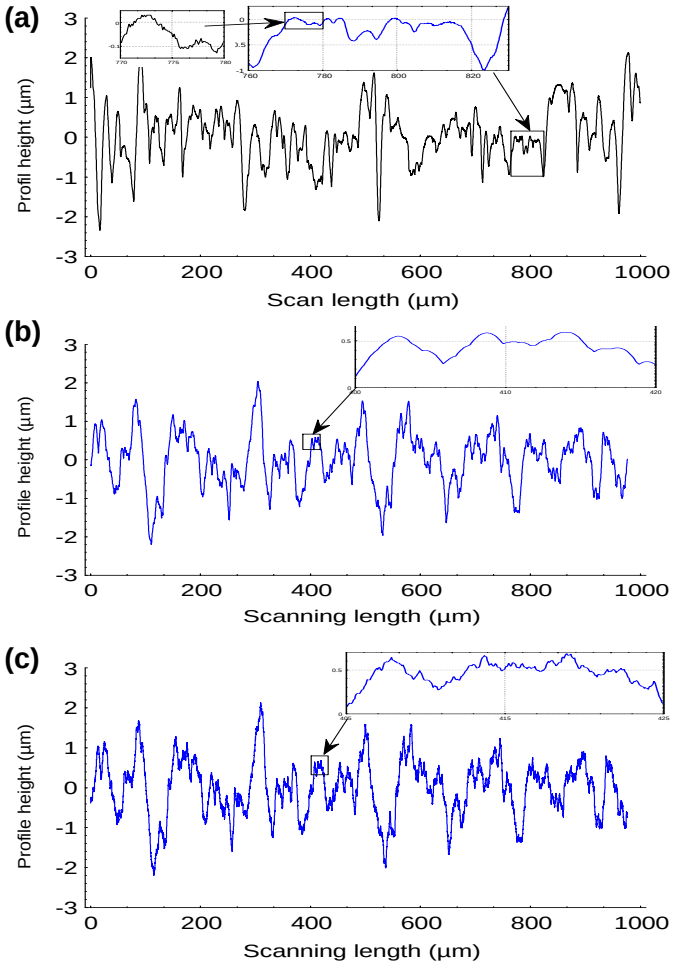

Figure 15: (a) Profile of a pure Aluminium sheet surface polished with paper grade 500 with a 10 µm stylus tip curvature. (b) Simulation of the scanning of the profile c with a 10 µm stylus tip curvature. (c) Simulation of profile a by stochastic circle function.

3.2.2 Fractal simulation of experimental measurements

We have decided to write an algorithm that simulates the stylus effect that we would apply to the Weirstrass functions defined only by an amplitude factor A and the Hölder exponent H (Eq. 19). This algorithm simulates physically the scanning effect without using mathematical considerations on the profile and it is then well adapted for fractal curves. By an inverse method, the scaling factor and the fractal dimension are adjusted to experimental data to reproduce profiles that look like the polishing profiles after the stylus scanning effect was simulated with a curvature radius of 10 µm. Figure 15b shows the simulated profile corresponding to the experimental one (Figure 15a) including the stylus integration simulation algorithm on the original simulated (Figure 15c). Table 1 presents the roughness parameters calculated on experimental profiles, as well as the simulated profiles and the stylus integration

simulation algorithm profiles (R_a: mean roughness amplitude, R_t: Range amplitude, *Peaks*: number of peaks by inch, *D*: fractal dimension calculated by the ANAM method [30, 31]).

Table 1: Comparison of roughness parameters calculated on measured and modelled profiles (R_a: mean roughness amplitude, R_t: total range amplitude, *Peaks*: number of peaks by inch, *D*: fractal dimension).

Roughness parameters	Measured r=10µm	Modelled r=10µm	Modelled r=0 µm
R_a (µm)	0.63	0.64	0.66
R_t (µm)	4.64	4.64	4.32
Peaks/inch	820	814	1186
D: Fractal dimension	1.08	1.09	1.23

From this analysis the following remarks can be stated:

i) Although our inverse method only use two parameters A and H, the experimental roughness parameters, the simulated ones and others are statistically equal. This point implies the following particular observations:

a) Our original fractal model is adequate for some complex worn surfaces such the polished ones with only two parameters. The mechanism seems then to be described by an amplitude phenomenon, a “circle base”, stochastic components and finally the fractal dimension.

b) The fractal dimension estimation calculated by the ANAM method seems to be very pertinent because when the estimated fractal dimension and the theoretical one are equal, the frequency roughness parameters are then equal.

ii) The Fractal dimension of simulated surfaces with stylus integration gives less information than the original one; stylus integration leads to see the surface more Euclidean than the reality, as a consequence of the smoothing effect. The under-estimation of surface fractal dimensions measured with a stylus is also confirmed by the decrease of the number of peaks characterizing a “less” fractal surface.

Published in Tribology International, Elsevier, Vol.65 (2013) p.235–247.
http://dx.doi.org/10.1016/j.triboint.2013.03.017

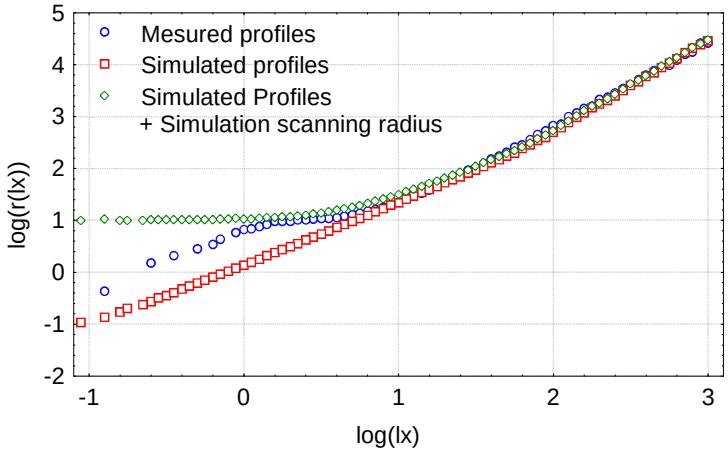

Figure 16: Evolution of the curvature radius $\log r\left(l_x\right)$ versus $\log l_x$ for profile shown in Figure 15a, Figure 15b and Figure 15c (l_x and $r(l_x)$ in µm).

iii) For a stylus radius not too-large (less than 10 µm), the amplitude parameters are quite constant. The stylus effect does not fundamentally destroy them. We then plot in Figure 16. $\log r_c\left(l_x\right)$ versus $\log l_x$ for the three categories of profiles (means values of 30 profiles). The following remarks will then be stated:

a) For $l_x > 30\ \mu m$, all points are confounded in a linear log-log relation meaning that:

1) There is no quantified stylus effect,

2) Models and simulated surfaces are similar in a great range of scale,

3) Hölderian and anti-Hölderian hypotheses on experimental profiles are respected.

b) Both simulated stylus and experimental profiles present a step at the value 10 µm that is exactly the curvature radius: our method allows us to detect the stylus effect and furthermore, allows us to quantify the curvature radius of the profiler. As consequence, this method then allows us to give the critical threshold concerning l_x and the value l_y under which the measurement effect could affect a metric value constructed on the signal. This aspect is a very important feature in the topographic measure area.

c) For the measured surface, if $l_x < 2\ \mu m$ the curvature radius increases linearly in the log-log plot with l_x. By analysing more precisely experimental data, it could be observed that a white noise due to the numeric analogical conversion with low amplitude is present in the profile. As we have shown in what precedes, this fact explains this linear tendency. The method proposed in this paper then allows us to detect high frequencies components and also to quantify the amplitude range for

Published in Tribology International, Elsevier, Vol.65 (2013) p.235–247.
http://dx.doi.org/10.1016/j.triboint.2013.03.017

which the measure could be influenced. We will now verify for different stylus radii the relation between the discretization steps related to the curvature radii of the profile and the stylus radius. All 100 profiles on which stylus integration algorithms are applied are then simulated. Curvature radii are so estimated by our method and Figure 17 shows this variation.

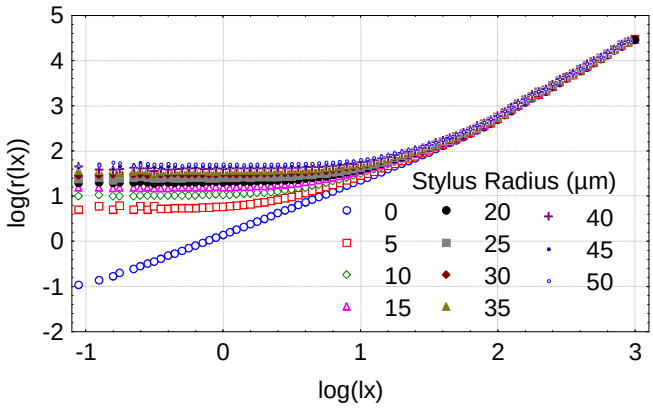

Figure 17: Evolution of the curvature radius $\log r\left(l_x\right)$ versus $\log l_x$ for profile shown in Figure 15c with different scanning simulation of the profiler stylus tip curvature varying in the range 0 to 100 µm (l_x and $r(l_x)$ in µm).

We then detect the step by taking only the radii values respecting the relationship $\log r_c\left(l_x\right) > 1 + \log l_x$ with $\log l_x < 1.5$.

On the other hand means values $r_c\left(l_x\right)$, called $r_c^T\left(\rho\right)$ are calculated for all values of l_x for each stylus radius ρ and $r_c^T\left(\rho\right)$ is so plotted versus ρ (Figure 18). By linear regression analyses, one then obtains:

$r_c^T\left(\rho\right) = 0.5_{\pm 1} + 1.014_{\pm 0.018}\,\rho$

with a correlation coefficient $r_{correl} = 0.9986$.

Published in Tribology International, Elsevier, Vol.65 (2013) p.235–247.
http://dx.doi.org/10.1016/j.triboint.2013.03.017

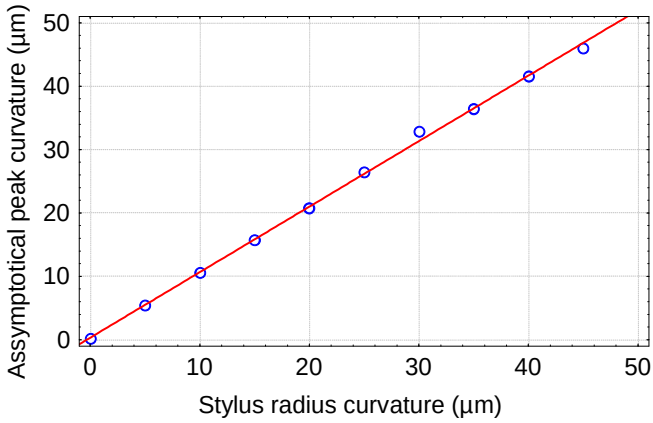

Figure 18: Plot of the asymptotic peak curvatures of Figure 17 versus the profiler stylus tip curvature.

4 Conclusions

A fractal approach of the curvature radius, on the basis of simulations, experimental measurements and analytical developments is presented in this paper. The proposed method generalizes the Nowicki's approach and then supplies a new tool overtaking the classic limits of the curvature radius analysis. It presents, in particular, an original advantage in the taking into account the highly non-linear stylus smoothing effect during the data gathering. New method is applied to tribological contact in metal forming process. Calculations of curvature radius along the tribological surface can be used to estimate the flattening effect of peaks curvature and therefore determine the areas of direct or boundary contact in measured tribological surfaces. This method can be of particular interest in lubricated contact to analyse lubrication regime and reveal the contact history. This technique showed to be robust in topographical contact analysis. Calculated average curvature of roughness peaks (r_c') can be used to estimate topographical signature of tribological contact.

5 Acknowledges

Authors would like to thank Prof. Niels Bay from Technical University of Denmark for providing experimental support for tribological drawing tests and stimulating scientific discussions.

K.J. Kubiak would like to thank Prof. L. Dubar, Prof. A Dubois and other members of staff of the Laboratory TEMPO at the University of Valenciennes for inviting him for 'visiting professorship', and very fruitful collaboration.

Published in Tribology International, Elsevier, Vol.65 (2013) p.235–247.
http://dx.doi.org/10.1016/j.triboint.2013.03.017

6 Appendix A. The Definition of a peak

We will now consider a peak as $z_{i-q} < ... < .z_{i-2} < z_{i-1} < z_i$ and $z_i > z_{i+1} > z_{i+2} > ... > z_{i+p}$, therefore $\tilde{l}_x = x_{i+p} - x_{i-q}$ and $\tilde{l}_y = z_i - (z_{i+p} + z_{i-q})/2$. It is then possible to compute a r_c value. With this formulation, peak will be seen as a non fractal structure. We will name this peak as Euclidian peak $\tilde{r}_c$. According to the Eq.23 by letting $\Delta = 1$ (non fractal structure), one would have $l_y(l_x) = \beta\, l_x$ and thus for any fractal dimension of the initial curve. This mean that giving an ideal definition of the radii curvature will pass over the fractal dimension of the curve and peaks become homothetic. We will now verify this assumption by simulate 1000 Brownian curves with a sampling length equal to unity and discretized in 4000 points. Amplitude of each curves are normalize to unity. Then we calculate the values of $\tilde{l}_x$, $\tilde{l}_y$ and $\tilde{r}_c$. We find the following relation $\tilde{l}_y = 30_{\pm 3}\tilde{l}_x^{1.01_{\pm 0.04}}$ with R=0.999 proving that this structure is Euclidean. In the Figure A1, we have plotted the evolution of the mean value of curvature radii calculated from the fractal (r_c), and non fractal approach ($\tilde{r}_c$) versus the values of l_x and $\tilde{l}_x$. Then regressions are proceeded on the two samples. The distribution of the number of peaks measured with the Euclidean method is plot on the Figure A1. One find the mean of $\tilde{l}_x$ equals to 4 and the number of $\tilde{l}_x$ decrease exponentially. On the fractal curve, the probability to have 99.5 % of detected radii $\tilde{r}_c$ by this classical algorithm are under 10 sampling length. The gravity centre of $\tilde{l}_y$ and $\tilde{r}_c$ is marked by the star on the graph. This point is on the curves of the fractal radii described by Eq. 22. What is then the physical meaning of that point? In fact, this Euclidian algorithm is only a particular case of our method. It fixe a critical length and measure all the homothetic peaks. This approach validates our original method of determination of radii curvature.

Published in Tribology International, Elsevier, Vol.65 (2013) p.235–247.
http://dx.doi.org/10.1016/j.triboint.2013.03.017

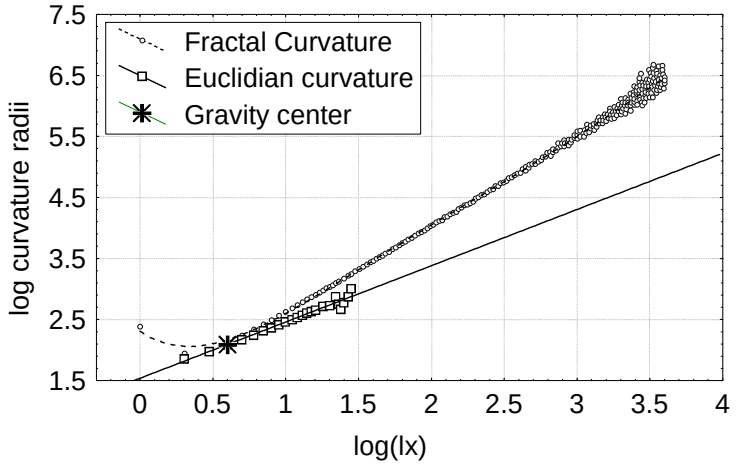

Figure A1: Evolution of the fractal radii curvature $\log r(l_x)$ and Euclidian radii curvature $\log \tilde{r}(l_x)$ versus $\log l_x$ for a Brownian motion.

7 Appendix B. Validation of the method on simulated fractal curves

To test the efficiency of our algorithm, we have chosen to calculate the curvature radius for curves with different fractal dimensions: a perfect white noise ($\Delta = 2$) and a Weierstrass Function with different fractal dimension.

7.1 The white noise

It seems not obvious to calculate a curvature radius for a white noise. In fact, we can find that R does not exist. We start from analysis of R properties: is R infinite? If that is the case, could the surface be considered as a plane? Is in this case the radius curvature $\tilde{r}_c$ still defined? How can we henceforth apply our reasoning to these two questions? In fact, that depends on the scale of observation. Indeed, according to Eq. 23, the condition allowing the definition of the curvature radius implies $l_x \geq \beta$ where β is a critical length where the peak is defined. Therefore, if $l_x < \beta$ neither $r_c(l_x)$ nor the relation $r_c(l_x) \propto l_x^{\Delta}$ are defined according to our formulation. On another hand, we obtain in this case $r_c(l_x) \propto l_y$ that seems coherent for a white noise. For that reason the curve appears as being more flat for a large scale of observations if its fractal dimension is high. It is particularly interesting to analyse the calculus of $\tilde{r}_c$ or r_c for a noise due to the following reasons: first, this noisy surface is a limit case in our study and the performance of our algorithm has to be tested, secondly, the recording devices could introduce white or pink noises that could influence the detection of the

curvature radius, and thirdly, we could analyse the probability to detect a peak that does not exist. We then apply our algorithm and plot the result in Figure B1. The following equation provides a good estimation of the fractal dimension $(\Delta = 2.005)$ with coefficient of regression r=0.99995.

$$\log r_c\left(l_x\right) = -0.914_{\pm 0.006} + 2.005_{\pm 0.002} \log l_x + 1.75_{\pm 0.01} / \left(n_x - 1\right) \quad \text{(b1)}$$

Where n_x is the number of d_x intervals used to calculate l_x. Without applying the discretization errors that are particularly important in the case of a white noise, one would have obtained the following equation:

$$\log r_c\left(l_x\right) = -0.4952 + 1.81 \log l_x \quad \text{(b2)}$$

with $\Delta = 1.81$ and with a 20 % error on the fractal dimension. Our modelling of the discretization error is then relatively efficient.

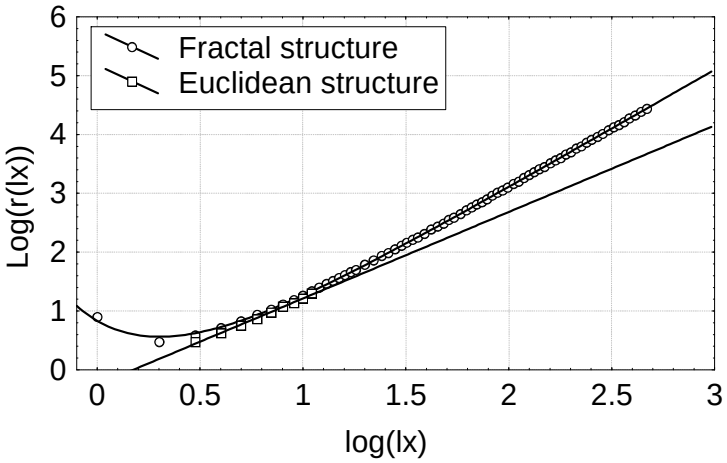

Figure B1: Evolution of the fractal curvature radius $\log r\left(l_x\right)$ and Euclidean curvature radius $\log \tilde{r}\left(l_x\right)$ versus $\log l_x$ for a white noise.

7.2 The fractional Brownian motion

The properties of a stochastic fractional Brownian motion (FBM) [24-25] allow us to determine the algorithm effect on the determination of r_c and $\tilde{r}$ for different fractal dimensions. The functions are determined by plotting different curves with different fractal dimensions (1 to 2 with 0.1 as discretization step). These curves are so discretized through 100000 points. Since the FBM realize stochastic curves, 100 curves are then simulated for each fractal dimension. Figure B2 shows the variation

of $\log\tilde{r}_c(l_x)$ (Euclidian peaks, see appendix A for mathematical definition) and $\log r_c(l_x)$ versus $\log l_x$ using the corrected method for 1, 1.2, 1.4, 1.6, 1.8 and 2 as theoretical fractal dimensions: first, Eq. b1 fit very well the experimental data for any fractal dimension. The greater the fractal dimension is, the more pertinent is the corrected method. One obtains for the correction coefficient α_2, $\alpha_2^{\Delta=1}=1.09$ $\alpha_2^{\Delta=1.2}=1.24$, $\alpha_2^{\Delta=1.4}=1.27$, and the following fractal dimensions $\Delta^{\Delta=1}=1.00$, $\Delta^{\Delta=1.2}=1.21$, , $\Delta^{\Delta=1.4}=1.40$, $\Delta^{\Delta=1.6}=1.58$, $\Delta^{\Delta=1.8}=1.75$ and $\Delta^{\Delta=2}=1.92$. The fractal dimension estimated from the radius curvature of the surface is well found whatever the theoretical fractal dimension is. Those results are coherent, as far as, the number of peaks in the l_x range decreases with the increase of the fractal dimension. For the Euclidean curve ($\Delta=1$, this curve is entirely differentiable), the regression lines of $\log\tilde{r}_c(l_x)$ and $\log r_c(l_x)$ versus $\log l_x$ are confounded. This means that both methods give the same estimation of the curvature radius for Euclidean curves. Since the fractal dimension increases, one obtains $\log\tilde{r}_c(l_x)<\log r_c(l_x)$ and the curvature radius is underestimated in the case of fractal curves, if we consider a peak as defined in Euclidian case (Appendix A). The difference increases with the fractal dimension confirming the hypothesis according to which, on the fractal curves, the peaks cannot be defined with the intuitive definition of the Euclidean curves.

Published in Tribology International, Elsevier, Vol.65 (2013) p.235–247.
http://dx.doi.org/10.1016/j.triboint.2013.03.017

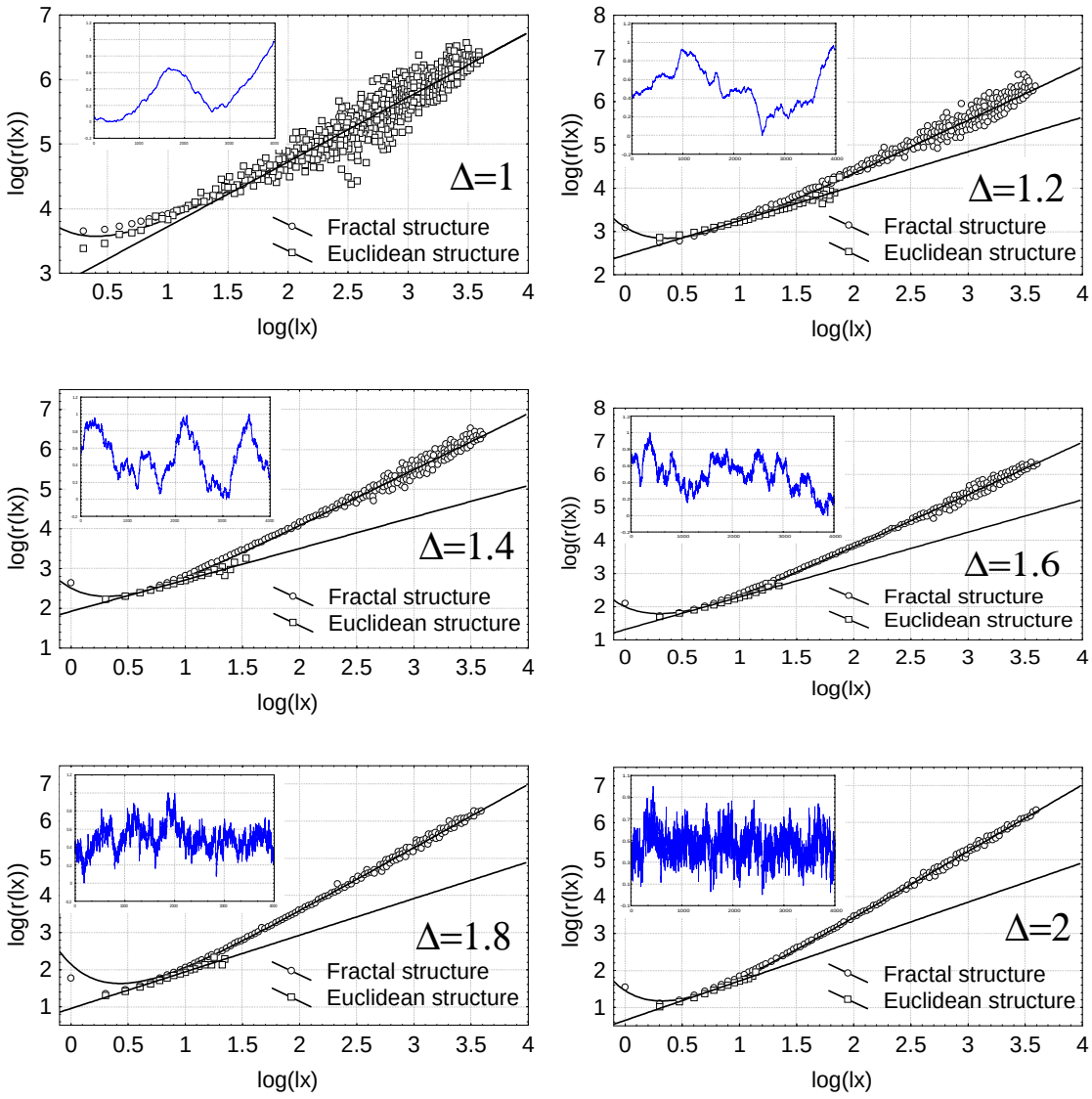

Figure B2: Evolution of the fractal curvature radius $\log r\left(l_x\right)$ and Euclidean curvature radius $\log \tilde{r}\left(l_x\right)$ versus $\log l_x$ for different fractional Brownian curves (fractal dimension 1, 1.2, 1.4, 1.6, 1.8, 2) with their associated profiles.

8 References

[1] Mandelbrot, B. B. and VAN NESS, J. W. 1968. Fractional Brownian motions, fractional noises and applications." SIAM Review: 422-437.

[2] Mandelbrot, B. B. and WALLIS, J. R. 1969. Computer experiments with fractal Gaussian noises. Part 1, averages and variances. Water Resources Research 10:228-241.

[3] M. Paggi, M. Ciavarella: The coefficient of proportionality k between real contact area and load, with new asperity models. Wear 268 (2010), p.1020-1029.

[4] M. Ciavarella, C. Murolo, G. Demelio: On the elastic contact of rough surfaces: Numerical experiments and comparison with recent theories, Wear 261 (2006), p.1101-1113.
[5] G. Zavarise, M. Borri-Brunetto, M. Paggi: On the resolution dependence of micromechanical contact models, Wear 262 (2007) p.42-54.
[6] J.-J. Wu: The properties of asperities of real surfaces. ASME Journal of Tribology, vol. 123, (2001), p.872-883.
[7] Ciulli E., Ferreira L.A., Pugliese G., Tvares S.M.O., Rough contact between actual engineering surfaces. Wear, vol.264 (2008), p.1105-1115.
[8] Nowicki, B. 1985. Multiparameter representation of surface roughness, Wear. 102:161-176.
[9] Whitehouse, D.J. Digital techniques, in rough surfaces (Ed. T.R. Thomas), 1982, 144-166 (Longman).
[10] Moalic, H. Fitzpatrick, J.A. Torrance, A.A. 1987. The correlation of the characteristics of rough surfaces with their friction coefficients, Proc. Instn Mech Engrs, 201:321-329.
[11] Thomas, T.R. 1975. Recent advances in the measurement and analysis of surface microgeometry, wear 33:205-233.
[12] Longuet-Higgins, M.S. 1957. Statistical properties of an isotropic random surface, Phil. Trans. R. Soc A 250:157-174.
[13] Whitehouse, D.J. and Archard, J.F. 1970. The properties of random surfaces of significance in their contact, Proc. R. Soc. A 316:97-121.
[14] Sayles, R.S. and Thomas, T. R. 1979. Measurements of the statistical microgeometry of engineering surfaces. Trans. ASME, J. Lubric. Technol. 101:409-418.
[15] Ganti, S., Bushan, B. 1995. Generalized fractal analysis and its applications to engineering surfaces, Wear:180:17-34.
[16] Gallant, J.C, Moore, I.D., Hutchinson, M.F. and Gessler, P. 1994. Estimating fractal dimension of profiles: A comparison of methods. Mathematical Geology:26:455-481.
[17] Hall, P. 1995. On the effect of measuring a self-similar process, SIAM, J. Appl. Math. 55:800-808.
[18] Amada, S. and Yamada, H. 1996. Introduction of fractal dimension to adhesive strength evaluation of plasma-sprayed coatings. Surface and Coatings Technology 78:50-55, 1996.
[19] Bozhelovny, S., B. Vohnsen. 1996. Fractal surface characterization: implications for plasmon polaritron scattering. Surface Science:356:268-274.
[20] Doege, E., Laackman, B., Kischnick, B. 1995. Characterisation of technical surfaces by means of fractal geometry. Steel research 66:113-116.
[21] Gagnepain, J. J. 1986. Fractal approach to two-dimensionnal and three-dimensionnal surface roughness. Wear 109:119-126.
[22] Tricot, C. 1995. Curves and Fractal Dimension, Springer.
[23] J. Bech, N. Bay, M. Eriksen, Entrapment and escape of liquid lubricant in metal forming, Wear 232 1999. 134–139.
[24] Dubar, L.; Hubert, C.; Christiansen, P.; Bay N., Dubois, A. Analysis of fluid lubrication mechanisms in metal forming at mesoscopic scale CIRP Annals - Manufacturing Technology, 2012, 61, 271 – 274.

[25] Poon, C. Y. and Bhushan, B. 1995. Comparison of surface roughness measurements by stylus profiler, AFM, and non-contact optical profiler, Wear. 190:76-88.
[26] Mc Cool, J. I. 1896. Comparison of models for the contact of rough surfaces, Wear. 107:37-60.
[27] Radhakrishnan, V. 1970. Effect of stylus radius on the roughness values measured with tracing stylus instruments, Wear 16:325-335.
[28] Whitehouse, D. J. 1974. Theoretical analysis of stylus integration, Ann. CIRP 23:181-182.
[29] Nakamura, T. 1966. On deformation of surface roughness curves caused by finite radius of stylus tip and tilting of stylus holder arm, Bul. Jap. Soc. Precision Eng. 1(4):240-248.
[30] Bigerelle, M. and Iost, A. 1996. Calcul de la dimension fractale d'un profil par la méthode des autocorrélations moyennées normées (AMN). C. R. Acad. Sci. Paris, 323, Série IIb:669-675.
[31] Bigerelle, M., Najjar, D. and Iost A. 2005. Multiscale functional analysis of wear a fractal model of the grinding process. Wear 258:232-239.